Journal of Alloys and Compounds 615 (2014) S348–S351

Contents lists available at ScienceDirect

Journal of Alloys and Compounds

journal homepage: www.elsevier.com/locate/jalcom

Compositional-induced structural change in Zr_xNi_{100-x} thin film metallic glasses

Matteo Ghidelli [a,b,c,*], Sébastien Gravier [a], Jean-Jacques Blandin [a], Thomas Pardoen [b], Jean-Pierre Raskin [c], Frédéric Mompiou [d]

[a] Science and Engineering of Materials and Processes, SIMaP, Université de Grenoble/CNRS, UJF/Grenoble INP, BP46, 38402 Saint-Martin d'Hères, France
[b] Institute of Mechanics, Materials and Civil Engineering, IMMC, Université catholique de Louvain, B-1348 Louvain-la-Neuve, Belgium
[c] Institute of Information and Communication Technologies, Electronics and Applied Mathematics, ICTEAM, Université catholique de Louvain, B-1348 Louvain-la-Neuve, Belgium
[d] CEMES-CNRS, Université de Toulouse, 29, rue J. Marvig, 31005 Toulouse, France

ARTICLE INFO

Article history:
Available online 15 December 2013

Keywords:
Metallic glasses
Thin films
Zr–Ni alloys
Atomic structure
Crystallization

ABSTRACT

The structure of Zr_xNi_{100-x} thin film metallic glasses (TFMGs) has been studied for a variety of compositions obtained by DC magnetron sputtering using a composite ZrNi target. The crystallization has been characterized by X-ray diffraction and transmission electron microscopy revealing also short and medium range order for amorphous compositions. The TFMGs thermodynamic stability has been evaluated by exploiting the Nagel and Tauc criterion, justifying the occurrence of crystallization in the Zr-rich specimens.

1. Introduction

Bulk metallic glasses (BMGs) are emerging materials with a unusual combination of superior properties involving a high fracture strength and large elastic deformation, wear and corrosion resistance as well as soft magnetic characteristics [1,2]. Thin film metallic glasses (TFMGs) have attracted recent attention due to additional interesting properties [3], but few studies have focused on the atomic structure of TFMGs and how this structure evolves when changing the film composition. Zr–Ni system is among the most studied bulk binary amorphous alloys, involving a high glass forming ability and a wide amorphisation range ($10 \leqslant$ Zr at.% $\leqslant 80$) [4]. The structure of Zr–Ni ribbons was firstly investigated by Buschow et al. and Dong et al. [4,5]. More recently, Liu and coworkers [6] investigated the local atomic structure in Zr–Ni metallic glasses ribbons using the extended X-ray absorption fine structure (EXAFS) technique, finding a strong chemical interaction between Zr and Ni atoms, hence a marked Short Range Order (SRO). Similar results have been also obtained by Fukunaga et al. [7] combining high resolution diffraction techniques and reverse Monte Carlo simulations. Direct evidence of SRO in $Zr_{66.7}Ni_{33.3}$ amorphous ribbons was reported by Hirata et al. [8], exploiting nano-beam electron diffraction and molecular dynamics simulation, with an icosahedral SRO as well as a strong correlation between Zr and Ni atoms.

The aim of this work is to investigate the evolution of the atomic structure of Zr–Ni films when varying the Zr composition between 42 and 85 at.%. The amorphous character of the films is studied by transmission electron microscopy (TEM) and X-ray diffraction (XRD). The Nagel and Tauc criterion [9] is applied for the determination of the (meta)stability of Zr–Ni TFMGs justifying the occurrence of crystallization for Zr-rich specimens.

2. Experiments

Zr_xNi_{100-x} (at.%) TFMGs have been deposited with a thickness of 800 nm on a clean silicon (100) substrate by means of DC–Magnetron sputtering (Alliance Concept AC450) within a class 1,000 clean room to limit sample contamination. The target-substrate distance was equal to 7 cm, while the background gas (Ar) pressure and DC-power were fixed to 0.3 Pa and 300 W, respectively. An original method for designing a composite sputtering target has been adopted in which pure grade Ni rectangular slices were inserted into a high purity Zr matrix to finely tune the film composition as well as to limit sample impurities. The composition of the films were checked at different locations over the wafer surface using energy dispersive X-ray spectroscopy (EDX) and electron probe micro-analysis (EPMA). The atomic structure was evaluated by XRD (Cu Kα radiation) and TEM (CM20 FEG, operating at 200 kV). In order to avoid perturbations from the Si (100) substrate, XRD measurements were performed in grazing incidence geometry. Cross-sectional TEM specimens were prepared by mechanical grinding and ion milling. Low voltage was used to avoid excessive heating. The film thickness was estimated by both mechanical profilometry and direct observations using field-emission scanning electron microscopy (FE-SEM), while the film density has been checked by X-ray reflectivity (XRR).

* Corresponding author at: Science and engineering of materials and processes, SIMaP, Université de Grenoble/CNRS, UJF/Grenoble INP, BP46 38402, Saint-Martin d'Hères, France. Tel.: +32 10472488, +33 476826465.
E-mail address: matteo.ghidelli@simap.grenoble-inp.fr (M. Ghidelli).

0925-8388/$ - see front matter © 2013 Elsevier B.V. All rights reserved.
http://dx.doi.org/10.1016/j.jallcom.2013.12.054

3. Results and discussion

The Ni concentration (C_{Ni}) which is a function of the number and width (l_{Ni}) of Ni slices inserted into the Zr matrix has been estimated considering the Zr and Ni sputtering yields (Y) and the maximum erosion circumference length (l_{tot}), using

$$\begin{cases} C_{Ni} = \frac{Y_{Ni} l_{Ni}}{Y_{Zr} l_{Zr} + Y_{Ni} l_{Ni}} \\ l_{tot} = l_{Ni} + l_{Zr} \end{cases} \quad (1)$$

The Ni and Zr sputtering yields have been determined for Ar^+ energy range between 400 and 1000 eV (corresponding to the imposed voltage), considering an incidence angle of 90° and neglecting any target topological effects. For the selected Ar^+ energies, the ratio Y_{Ni}/Y_{Zr} is constant and is equal to 2.

Four compositions have been selected, i.e. $Zr_{48}Ni_{52}$, $Zr_{70}Ni_{30}$, $Zr_{80}Ni_{20}$ and $Zr_{90}Ni_{10}$, by inserting respectively, 12, 6, 4, and 2 Ni slices in the target. As shown in Table 1, the EDX and EPMA film composition analyses are slightly richer in Ni, namely $Zr_{42}Ni_{58}$, $Zr_{65}Ni_{25}$, $Zr_{75}Ni_{25}$ and $Zr_{85}Ni_{25}$ (at.%) with respect to the theoretical calculation. The discrepancy has been attributed to sputtering events outside the maximum erosion circumference not considered by the model underlying Eq. (1). The film composition is found constant over the entire surface, which is a sign of a uniform and efficient plasma mixing with a negligible amount of C and O. All samples used for further analysis are extracted from the center region with a thickness around 800 nm.

The XRD diffractograms of Zr_xNi_{100-x} TFMGs in Fig. 1a are provided for the compositions lying within the theoretical amorphisation range ($10 \leqslant$ Zr at.% $\leqslant 80$), namely $Zr_{42}Ni_{58}$, $Zr_{65}Ni_{35}$ and $Zr_{75}Ni_{25}$. As expected for amorphous materials which have no long-range periodicity [10], an asymmetric First Sharp Diffraction Peak (FSDP) centered between 35° and 40° is observed followed by a second broader halo around 65°. If the 2θ output is converted into scattering vector coordinate (q, $Å^{-1}$) by means of $q = 4\pi \sin\theta/\lambda$ and if a Lorentzian fit is applied, a full width at high maximum (FWHM) between 0.30 $Å^{-1}$ and 0.42 $Å^{-1}$ increasing with the Ni content in the film is found for the FSDP, slightly below the literature results for amorphous bulk alloys (0.40–0.5 $Å^{-1}$) [11]. According to Chou et al. [12] who investigated the atomic structure for ternary Zr–-Cu–Ti BMGs, an increment of the FWHM with Ni content is an indication of an increase of structural disorder (so called *confusion* principle [13]). Nevertheless, a strong atomic correlation clearly exists since the obtained values are lower than the literature data in the case of multi-components BMGs [11].

Furthermore, the position of the FSDP (Q_p) is shifted toward lower scattering angles (θ) when increasing the amount of Zr in the film, from 2.52 $Å^{-1}$ up to 2.80 $Å^{-1}$ for $Zr_{75}Ni_{25}$ and $Zr_{42}Ni_{58}$, respectively. These results are in a good agreement with the Q_p variation reported by Buschow et al. [4] for Zr–Ni amorphous ribbons, for which the Q_p linearly decreases for Zr-rich specimens (see Fig. 3). Such a results could be easily related to the favored formation of strong hetero Zr–Ni bonds when the content of Ni increases in the film leading to an increment of the cohesive energy and a

Table 1
TFMGs composition as function of the number of Ni slices in the target. The expected composition deduced from Eq. (1) and the measured one using electron probe microanalysis (EPMA) and energy dispersive X-ray spectroscopy (EDX) are shown.

Number of Ni slices within the target	Expected composition (% at.)	EPMA composition (% at.)	EDX composition (% at.)
12	$Zr_{48}Ni_{52}$	$Zr_{42}Ni_{58}$	$Zr_{44}Ni_{56}$
6	$Zr_{70}Ni_{30}$	$Zr_{65}Ni_{35}$	$Zr_{68}Ni_{32}$
4	$Zr_{80}Ni_{20}$	$Zr_{75}Ni_{25}$	$Zr_{75}Ni_{25}$
2	$Zr_{90}Ni_{10}$	$Zr_{85}Ni_{15}$	$Zr_{86}Ni_{14}$

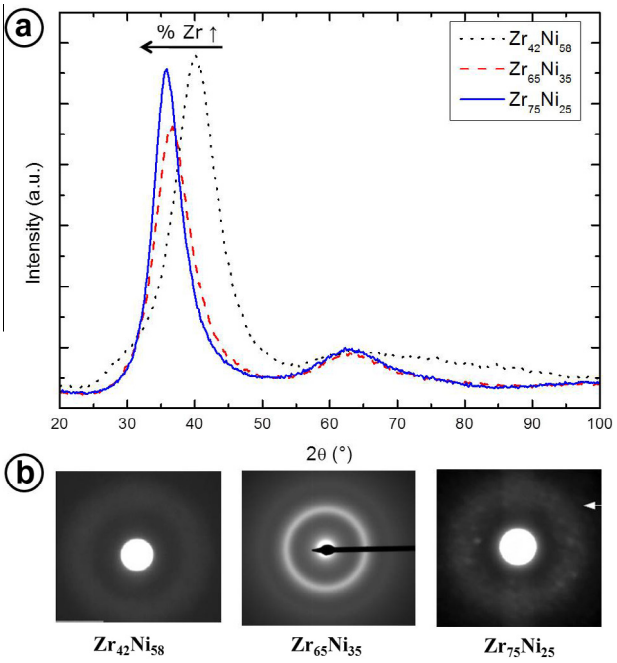

Fig. 1. (a) XRD diffractograms for different Zr_xNi_{100-x} TFMGs, a First Sharp Diffraction Peak (FSDP, around 35°–40°) and a second broader peak at higher θ angles is observed for all compositions. The position of the FSDP is shifted toward lower angles when increasing the Zr percentage in the film. (b) TEM micro-diffraction patterns for different compositions, a speckle (white arrow) is found for $Zr_{75}Ni_{25}$ indicating the formation of nano-crystals (~3 nm).

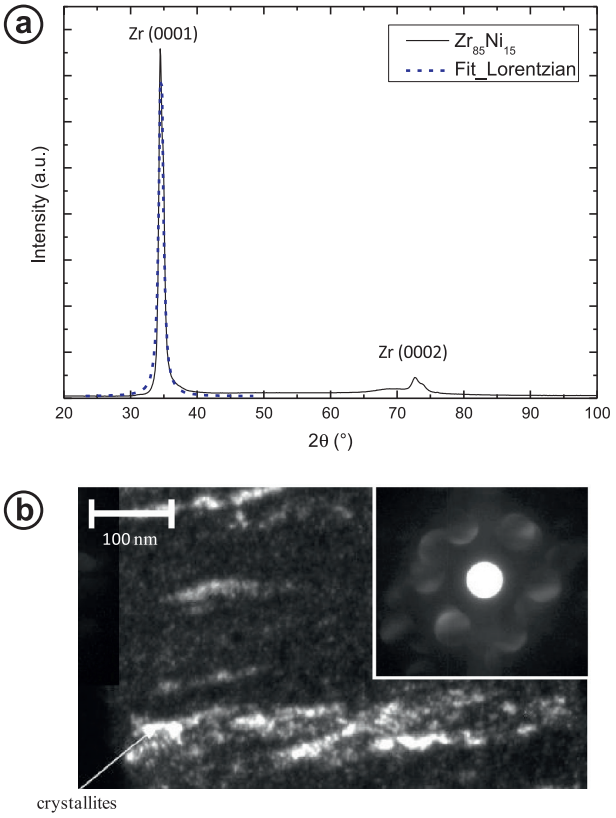

Fig. 2. (a) XRD diffractograms of $Zr_{85}Ni_{15}$ TFMG in which the crystalline α-Zr peaks corresponding to family plane (0001) are clearly visible at 34.5°, (b) TEM cross-section images and micro-diffraction patterns highlighting the presence of long α-Zr crystalline phase.

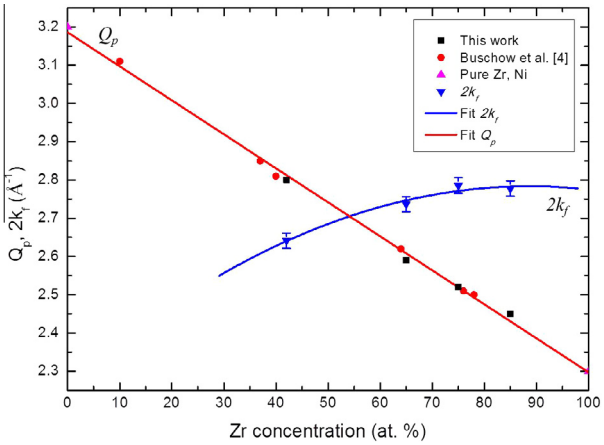

Fig. 3. Variation of the position of the First Sharp Diffraction Peak (FSDP, Q_p) and of the Fermi wavevector ($2k_f$) as function of film composition. Black squares and red circles indicate, respectively, the position of the FSDP measured for TFMGs and the values obtained by Buschow et al. [4] for amorphous Zr–Ni ribbons. A maximum of (meta)stability is found around 54% of Zr ($Q_p = 2k_f$).

reduction of the average atomic distance as well [14]. For instance, the atomic radii of Zr and Ni are 160 pm and 124 pm, respectively. Moreover, if the atomic volume (V_a, Å^3) – defined for an amorphous alloys as $V_a = \bar{A}/(\rho N_a)$ [11] where $\bar{A}$ is the weighted atomic mass, ρ is the density, and N_a is the Avogadro number – is calculated for different film compositions, a linear variation of Q_p is found inversely proportional to V_a. This correlation follows the trend obtained by Ma et al. [11], for different families of BMGs, i.e., more precisely, the relationship $Q_p \cdot V_a^{0.433\pm0.007} = 9.3 \pm 0.2$. Therefore, according to Ma and coworkers [11], since the power-law scaling coefficient is higher than 1/3, a short (~0.5 nm) and medium range order (MRO, 0.5–2 nm) can be deduced for Zr_xNi_{100-x} TFMGs. This result emerges from the direct analysis of the X-ray diffractograms as well (Fig. 1a) in which a FSDP is followed by a second larger halo, indicating a strong correlation at least within the first and the second neighbor shells from a selected atom. Moreover, both SRO and MRO for these compositions are expected because of the high negative mixing enthalpy and Gibbs free energy as well, with a maximum around 40–50 at.% of Zr that favors Zr–Ni atomic bonds [15].

Fig. 1b reports the electron micro-diffraction images obtained by TEM. Considering first the compositions $Zr_{42}Ni_{58}$ and $Zr_{65}Ni_{35}$, the presence of diffuse halos agrees with the presence of a FSDP followed by a second broad peak shown in X-ray diffractograms in Fig. 1a. Again, these features indicate a strong local order for these compositions. The halo width – enhanced for the composition $Zr_{42}Ni_{58}$ – is in agreement with the large FWHM found in the XRD experiments. For the $Zr_{75}Ni_{25}$ composition, a speckle is found (white arrow) within the characteristic diffuse halo. The speckle is a fingerprint of the formation of nano-crystals whose average size is estimated to be around 3 nm. This feature is not observed during XRD experiments due to the lower spatial resolution. Nevertheless, the origin of these dispersed nano-crystals is not unexpected since the composition is close to the limit of the amorphisation interval ($10 \leqslant$ Zr at.% $\leqslant 80$) and the value of mixing enthalpy and Gibbs free energy is significantly reduced [15]. It is speculated that the composition of the nano-crystals is a Zr-rich phase (α-Zr or Zr_2Ni) as expected from the Zr–Ni equilibrium phase diagram [15]. Nevertheless, the small size of the nano-crystals did not allow a clear identification of this phase.

The X-ray diffractogram of $Zr_{85}Ni_{15}$ TFMGs is reported in Fig. 2a. Contrary to what has been shown in Fig. 1a, a standard Bragg–Brentano configuration has been exploited for the XRD experiments. An offset equal to 2° between the X-ray source and the detector has been imposed to limit the Si substrate signal. This configuration makes possible the detection of the crystalline phase without the formation of shifted Bragg peaks arising from a grazing angle geometry. Nevertheless, a Si signal is still visible at 2θ angle around 69°. The analysis of Fig. 2a reveals the presence of a crystalline phase. In particular, the position of the first Bragg diffraction peak at 34.5° corresponds to the family plane (0001) for a crystalline hexagonal α-Zr. The absence of other diffraction peaks in Fig. 2a indicates that the vertical *c* axis of the hexagonal lattice is oriented normal to the Si surface. A further proof of this crystalline structure is the presence of the (0002) fringe around 72°. Furthermore, if a grazing angle configuration is adopted to analyze this composition (not reported here) the combined presence of large peaks (characteristic of an amorphous phase) is observed as well as Bragg peaks. Therefore, a composite structure in which a crystalline phase is embedded within an amorphous matrix is expected. Fig. 2b shows a dark field image obtained with one of the diffracted beam (inset of Fig. 2b) with clear evidences of long nano-crystals (length of 60–70 nm and width around 4–5 nm) oriented normal to the Si surface (in agreement with XRD). The presence of the amorphous phase can be inferred from the low intensity diffuse halo with a spherical symmetry visible in the electron micro-diffraction pattern (see the inset in Fig. 2b). The formation of a crystalline phase is expected since the selected composition is outside the amorphisation range for Zr–Ni alloys ($10 \leqslant$ Zr at.% $\leqslant 80$) and the mixing stabilizing energy contribution is significantly reduced [15]. It has been proven that this amorphisation domain is also achieved for thin films deposited by a vapor phase technique. We suppose that, although the cooling rate imposed by sputtering is very high, the large amount of Zr in the film favor crystallization phenomena with a lower energy content. In other words, the "*confusion* principle" usually considered for the formation of amorphous alloys [13] is not completely fulfilled, thus leading to the nucleation of a crystalline phase.

The analysis of TFMGs (meta)stability is reported in Fig. 3 on the basis on the Nagel and Tauc criterion [9]. This criterion has been validated in the case of binary metal–metalloid amorphous alloys AuP and AuSi [9] and it has been successfully adopted by Buschow et al. [4] for Zr–Ni and Zr–Co ribbons as well as by Chen et al. [16] in the case of Zr–Al–Ni–Cu BMGs. This criterion states that when Q_p – the scattering vector corresponding to the FSDP – is equal to $2k_f$ (twice the Fermi wavevector), then an energy gap opens between the valence and conduction bands. This mechanism is associated with a stabilization of the glassy structure. While Q_p can be obtained after a Lorentzian fit of the FSDP, k_f is calculated as proposed by Buschow et al. [4] and Chen et al. [16] as

$$k_f = \left(\frac{3\pi^2 N_a \rho \bar{Z}}{\bar{A}}\right)^{1/3} \quad (2)$$

where $\bar{A}$ and $\bar{Z}$ are the weighted atomic mass and the effective valence, respectively. As proposed by Buschow et al. [4], the atomic valence is considered equal to 0.6 for Ni and of 2 for Zr. The film density ρ is deduced from XRR experiments, contrary to [4] who estimated the Zr–Ni ribbons density on the basis of a weighted mixing rule, without taking into account the presence of a SRO and MRO that increase the effective density value. Fig. 3 shows that the maximum (meta)stability corresponds to the $Zr_{54}Ni_{46}$ composition, in agreement with the maximum negative mixing enthalpy and Gibbs free energy for Zr–Ni binary systems [15] due to the formation of Zr–Ni hetero bonds, thus further justifying the XRD analysis previously exposed. Moreover, for TFMGs with a composition for which $2k_f \gg Q_p$ (namely $Zr_{75}Ni_{25}$ and $Zr_{85}Ni_{15}$) it is expected a low (meta)stability, thus justifying the occurrence of crystallization phenomena.

4. Conclusion

In summary, we investigated the atomic structure of Zr_xNi_{100-x} thin film metallic glasses (TFMGs) produced by magnetron sputtering. The compositional control has been successfully achieved by the development of an innovative composite target in which Ni slices are inserted into a Zr matrix. A model describing the Zr–Ni bonds formation, increasing the Ni percentage in the film has been developed, highlighting the presence of a SRO and MRO. Crystallization has been observed for Zr-rich specimens at the edge or outside the amorphisation range, and a crystalline α-Zr phase has been clearly identified.

Acknowledgments

The authors thank the PTA (Plateforme Technologique Amont) for deposition facilities, Stéphane Coindeau and Gregory Abadias for the XRD and XRR analyses, respectively. M.G. gratefully acknowledges the financial support of the Erasmus Mundus program in functional materials (FunMat). This work has been carried out in the framework of the Belgian Science Policy through the IAP 7/21 project.

References

[1] M. Ashby, A. Greer, Scr. Mater. 54 (2006) 321–326.
[2] A. Inoue, A. Takeuhi, Mater. Trans. 43 (2002) 1892–1906.
[3] J.P. Chu, J.S.C. Jang, J.C. Huang, H.S. Chou, Y. Yang, J.C. Ye, Y.C. Wang, J.W. Lee, F.X. Liu, P.K. Liaw, Y.C. Chen, C.M. Lee, C.L. Li, C. Rullyani, Thin Solid Films 520 (2012) 5097–5122.
[4] K.H.J. Buschow, N.M. Beekmans, Phys. Rev. B: Condens. Matter 19 (1979) 3843–3849.
[5] Y.D. Dong, G. Gregan, M.G. Scott, J. Non-Cryst. Solids 43 (1981) 403–415.
[6] X.J. Liu, X.D. Hui, G.L. Chen, T. Liu, Phys. Lett. A 373 (2009) 2488–2493.
[7] T. Fukunaga, K. Itoh, T. Otomo, K. Mori, M. Sugiyama, H. Kato, M. Hasegawa, A. Hirata, Y. Hirotsu, A.C. Hannon, Intermetallics 14 (2006) 893–897.
[8] A. Hirata, P. Guan, T. Fujita, Y. Hirotsu, A. Inoue, A.R. Yavari, T. Sakurai, M. Chen, Nat. Mater. 10 (2010) 28–33.
[9] S.R. Nagel, J. Tauc, Phys. Rev. Lett. 35 (1975) 380–383.
[10] H.W. Sheng, W.K. Luo, F.M. Alamgir, J.M. Bai, E. Ma, Nature 439 (2006) 419–425.
[11] D. Ma, A.D. Stoica, X-L. Wang, Nat. Mater. 8 (2009) 30–34.
[12] H.S. Chou, J.C. Huang, L.W. Chang, T.G. Nieh, Appl. Phys. Lett. 93 (2008) 191901.
[13] A.L. Greer, Science 267 (1995) 1947–1953.
[14] R. Ristić, M. Stubičar, E. Babić, Philos. Mag. 87 (2007) 5629–5637.
[15] A.I. Zaitsev, N.E. Zaitseva, E.K. Shakhpazova, A.A. Kodentsov, Phys. Chem. Chem. Phys. 4 (2002) 6047–6058.
[16] W. Chen, Y. Wang, J. Qiang, C. Dong, Acta Mater. 51 (2003) 1899–1907.